Journal of Solid State Chemistry 184 (2011) 411–418

Contents lists available at ScienceDirect

Journal of Solid State Chemistry

journal homepage: www.elsevier.com/locate/jssc

Preferential growth orientation of laser-patterned $LiNbO_3$ crystals in lithium niobium silicate glass

T. Komatsu *, K. Koshiba, T. Honma

Department of Materials Science and Technology, Nagaoka University of Technology, 1603-1 Kamitomioka-cho, Nagaoka 940-2188, Japan

ARTICLE INFO

Article history:
Received 14 October 2010
Received in revised form
8 December 2010
Accepted 12 December 2010
Available online 21 December 2010

Keywords:
Laser pattering
Glass
$LiNbO_3$
Preferential orientation
Micro-Raman spectrum

ABSTRACT

Dots and lines consisting of $LiNbO_3$ crystals are patterned on the surface of $1CuO–40Li_2O–32Nb_2O_5–28SiO_2$ (mole ratio) glass by irradiations of continuous-wave Nd:YAG laser (wavelength: $\lambda=1064$ nm), diode laser ($\lambda=795$ nm), and Yb:YVO_4 fiber laser ($\lambda=1080$ nm), and the feature of laser-patterned $LiNbO_3$ crystal growth is examined from linearly polarized micro-Raman scattering spectrum measurements. $LiNbO_3$ crystals with the *c*-axis orientation are formed at the edge parts of the surface and cross-section of dots. The growth direction of an $LiNbO_3$ along the laser scanning direction is the *c*-axis. It is proposed that the profile of the temperature distribution in the laser-irradiated region and its change along laser scanning would be one of the most important conditions for the patterning of crystals with a preferential growth orientation. Laser irradiation giving a narrow width is also proposed to be one of the important factors for the patterning of $LiNbO_3$ crystal lines with homogeneous surface morphologies.

1. Introduction

Laser microfabrication or micromachining in materials is now an important technique for many high technology devices [1]. Recently, laser-induced crystallization of glass has received much attention, because laser irradiation is regarded as a process for spatially selected patterning of functional crystals on the glass substrates [2–7]. For instance, lines with highly oriented nonlinear optical crystals such as β-BaB_2O_4 and β′-$Gd_2(MoO_4)_3$ have been patterned successfully by just scanning of continuous-wave (cw) Nd:YAG laser (wavelength: $\lambda=1064$ nm) or Yb:YVO_4 fiber laser ($\lambda=1080$ nm) [8–11]. Phenomena taking place in the laser-irradiated region in glass depend on laser irradiation conditions, i.e., wavelength, power, irradiation time, scanning speed, and on the properties of a given glass, i.e., glass composition, glass transition temperature, crystallization temperature, thermal conductivity, etc., and thus, the mechanism of laser-induced crystallization in glass would be different in each case. Indeed, different morphologies have been observed in crystals patterned by laser irradiations [2–11].

Lithium niobate $LiNbO_3$ is an important ferroelectric and has been used in various applications such as surface acoustic wave devices and phase modulator waveguides in integrated optics, due to its excellent electro-optical and photorefractive properties. It is, therefore, of particular interest and of importance to pattern highly oriented $LiNbO_3$ in glasses. The laser-induced crystallization technique has been applied to the formation of an $LiNbO_3$ in glasses [12–15], and lines consisting of highly oriented $LiNbO_3$ crystals have been successfully patterned. At this moment, however, an information on the crystal growth mechanism in the laser-induced crystallization and the effect of laser-type used on the morphology of crystal dots and lines are limited. Laser patterning of $LiNbO_3$ crystals would be a good model for the understanding of the feature (e.g., orientation and growth mechanism) of laser-patterned crystals in glass in detail.

In this study, we patterned dots and lines consisting of $LiNbO_3$ crystals on the surface of $1CuO–40Li_2O–32Nb_2O_5–28SiO_2$ glass using the laser-induced crystallization method, i.e., transition metal atom heat (TMAH) processing, and clarified the feature of the preferential orientation of laser-patterned $LiNbO_3$ crystals. Three different lasers of Nd:YAG laser ($\lambda=1064$ nm), diode laser ($\lambda=795$ nm), and Yb:YVO_4 fiber laser ($\lambda=1080$ nm) were used. In TMAH processing for the present glass, irradiated lasers are absorbed by Cu^{2+} ions through *d–d* transitions, and the laser energy absorbed is transferred to the lattice system (lattice vibrations) through a non-radiative relaxation process (electron–phonon couplings). And thus the surrounding of Cu^{2+} ions is heated, consequently inducing crystallizations in the glass.

2. Experimental

Two glasses with and without CuO were prepared in this study. That is, one is $40Li_2O–32Nb_2O_5–28SiO_2$ glass (mol%) (designated here as an LNS glass) and $1CuO–40Li_2O–32Nb_2O_5–28SiO_2$ glass (mole ratio) (Cu–LNS glass). The latter is equal to the composition

* Corresponding author. Fax: +81 258 47 9300.
E-mail address: komatsu@mst.nagaokaut.ac.jp (T. Komatsu).

0022-4596/$ - see front matter © 2010 Elsevier Inc. All rights reserved.
doi:10.1016/j.jssc.2010.12.016

of 0.99CuO–39.6Li_2O–31.69Nb_2O_5–27.72SiO_2 (mol%). These glasses were prepared using a conventional melt quenching method. Commercial powders of reagent grade Li_2CO_3, Nb_2O_5, SiO_2, and CuO were mixed and melted in a platinum crucible at 1300 °C for 1 h in air in an electric furnace. The melts were poured onto an iron plate and pressed to a thickness of ~1 mm with another iron plate. The glass transition, T_g, and crystallization peak, T_p, temperatures were determined using differential thermal analyses (DTA) at a heating rate of 10 K/min.

The as-quenched glasses were annealed at T_g for 30 min to release internal stresses and mechanically polished to a mirror finish with diamond slurries. Optical absorption spectra for the annealed glasses were measured in the wavelength range 200–2000 nm, using a spectrometer (Shimadzu: UV-3150). Densities of glasses were determined with Archimedes method, using distilled water as an immersion liquid. The glasses were heat-treated at different temperatures (590–900 °C) in an electric furnace, and crystalline phases present in the heat-treated samples were examined by X-ray diffraction (XRD) analyses (Cu $K\alpha$ radiation) at room temperature. Second harmonic (SH) intensities of the crystallized samples were measured by using a fundamental wave of a Q-switched Nd:YAG laser with $\lambda=1064$ nm as a function of the angle of an incident light, i.e., Maker fringe method. As a polarization on SH intensity measurements, the combination of *p*-excitation and *p*-detection (*pp* polarization) was used.

Cw Nd:YAG laser with $\lambda=1064$ nm, diode laser (LD) with $\lambda=795$ nm, and Yb:YVO_4 fiber laser with $\lambda=1080$ nm were used for the formation of dots and lines consisting of $LiNbO_3$ crystals. Surface of polished glasses were irradiated by lasers. For the patterning of lines, the sample was mechanically moved during the laser irradiation with some translation speeds such as $S=5$ μm/s. The dots and lines with structural changes were observed with polarization optical (OLYMPUS: BX51) and confocal scanning laser microscopes (OLYMPUS: OLS 3000), and micro-Raman scattering spectra (Tokyo Instruments Co., Nanofinder; Ar^+ laser 488 nm).

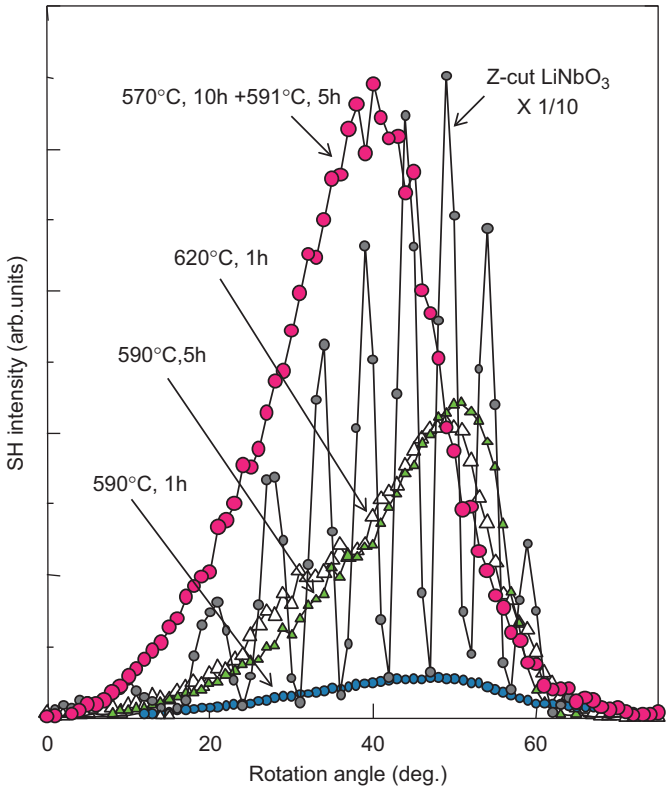

Fig. 1. Maker fringe patterns in the rotation angle of 0–70° for some optically transparent crystallized LNS glasses consisting of an $LiNbO_3$.

3. Results and discussion

3.1. Features of precursor glasses and crystallized samples

In order to study the preferential growth orientation of $LiNbO_3$ crystals patterned by laser irradiations in a given glass (precursor glass), it would be worth to understand the crystallization behavior of the precursor glass in an electric furnace in advance. So far, many studies on the fabrication of crystallized glasses consisting of $LiNbO_3$ crystals have been reported [16–26]. Although the formation mechanism of $LiNbO_3$ crystals depends on the glass system, glass composition, and heat treatment temperature, it has been recognized that there are some important features: the phase separation is taking place prior to the crystallization of an $LiNbO_3$, randomly oriented $LiNbO_3$ nano-crystals are dispersed in the glass matrix, textured layers of $LiNbO_3$ crystals are formed at the glass surface, and second harmonic generations (SHGs) have been observed from some crystallized glasses with an $LiNbO_3$. In this section, we describe some features of LNS (40Li_2O–32Nb_2O_5–28SiO_2) and Cu–LNS (1CuO–40Li_2O-32Nb_2O_5–28SiO_2) glasses and crystallized samples.

The samples of LNS and Cu–LNS, prepared in this study, showed only halo patterns in XRD patterns. The endothermic peaks, due to the glass transition and exothermic peaks, due to the crystallization, were observed in the DTA curves for both glasses, giving the values of $T_g=560$ and $T_p=694$ °C for an LNS glass and $T_g=544$ and $T_p=692$ °C for the Cu–LNS glass. The densities (*d*) of LNS and Cu–LNS glasses at

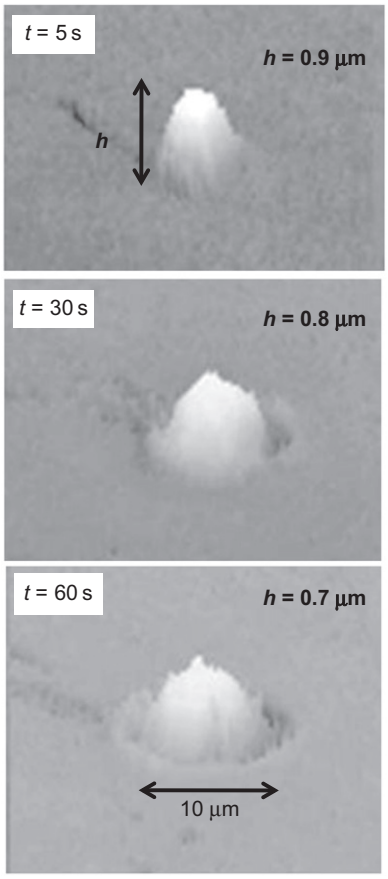

Fig. 2. Confocal scanning laser microscope observations for the samples obtained by Nd:YAG laser ($\lambda=1064$ nm) irradiations with a laser power of $P=0.5$ W and irradiation times, *t*, of $t=5$, 30, and 60 s in the Cu–LNS glass.

room temperature were found to be $d=3.772$ and 3.771 g/cm^3, respectively. As reported by Honma et al. [27], an LNS glass with no CuO addition is colorless in the visible light region, and CuO-added glass shows green color, giving a strong and broad absorption peak at ~800 nm, in the optical absorption spectra, at room temperature. It was also observed that the absorption edge shifts towards longer wavelength, due to the addition of CuO. The broad peak at ~800 nm is assigned to the $^2B_{1g}\rightarrow{}^2B_{2g}$ transition in Cu^{2+} ions in octahedral sites with strong tetrahedral distortions [28,29], and the shift would be assigned to the transition of $3d^{10}\rightarrow 3d^9 4s$ in Cu^+ ions [30]. It is, therefore, concluded from the optical absorption spectra that both Cu^+ and Cu^{2+} ions are present in the Cu–LNS glass. The absorption coefficients (α) at the wavelengths of $\lambda=795$ nm (LD laser), $\lambda=1064$ nm (Nd:YAG laser), and $\lambda=1080$ nm (Yb:YVO_4 laser) for Cu–LNS glass were evaluated to be $\alpha=7.19$, 2.91, and 2.72 cm^{-1}, respectively.

LNS and Cu–LNS glasses were heat-treated at different temperatures (590–900 °C) for 1 h in air, and it was confirmed from XRD patterns that $LiNbO_3$ crystals are formed. In particular, it was found that the relative intensity of the peak corresponding to the (0 0 6) plane increases with an increasing heat treatment temperature and the peak intensity of the (0 1 2) plane is extremely small. The crystallized samples obtained by heat-treatments at 590 and 620 °C were transparent, but the samples heat-treated at 670, 720, and 900 °C were opaque. It is, therefore, concluded that $LiNbO_3$ crystals tend to show orientations at the surface of the heat-treated samples. Sigaev et al. [24] have reported the textured layer of $LiNbO_3$ crystals at the surface of crystallized (600–650 °C, 1 h) samples in $30Li_2O$–$25Nb_2O_5$–$45SiO_2$ glass. Ding et al. [18] also reported the surface crystallized (610 °C, 3 h) glasses with partially c-axis oriented $LiNbO_3$ fine grains in $35Li_2O$–$30Nb_2O_5$–$35SiO_2$ glass.

Maker fringe patterns in the rotation angle of 0–70° for some optically transparent crystallized (590, 620 °C, 1 h) LNS glasses consisting of an $LiNbO_3$ are shown in Fig. 1. The sample obtained by two-step heat treatment (570 °C, 10 h+591 °C, 5 h) was also prepared. In Fig. 1, Maker fringe pattern for Z-cut $LiNbO_3$ single crystal is also included. It is seen that transparent crystallized glasses show second harmonic generations (SHGs) clearly. In particular, it is noted that the sample obtained by the two-step heat treatment gives a strong SH intensity close to one tenth of the SH intensity of an $LiNbO_3$ single crystal. The results obtained in the present study suggest that Cu–LNS glass with the composition of $1CuO$–$40Li_2O$–$32Nb_2O_5$–$28SiO_2$ would be a good example for the study of the preferential growth orientation and growth mechanism of laser-patterned $LiNbO_3$ crystals.

3.2. Growth of $LiNbO_3$ crystal dots by laser irradiation

The confocal scanning laser microscope (CSLM) observations for the samples obtained by Nd:YAG laser irradiations with a laser power of $P=0.5$ W and irradiation times, t, of $t=5$, 30, and 60 s in the Cu–LNS glass are shown in Fig. 2. It is seen that structural changes are induced by laser irradiations. The size of the dots is about 10 μm, and bumps with a height of 0.7–0.9 μm are formed. It is noted that with increasing laser irradiation time, the formation of sinkings are observed at the surrounding of dots. The micro-Raman scattering spectra at room temperature for these dots are shown in Fig. 3 together with the data for the base Cu–LNS glass (no laser irradiations) and $LiNbO_3$ crystal powders. It is seen that the Raman spectra for the dots obtained by laser irradiations of $t=30$ and 60 s are almost the same as that for $LiNbO_3$ crystals. On the other hand, the dot obtained with $t=5$ s has no sharp Raman peak, as similar to the base glass. A similar behavior was observed in the condition of

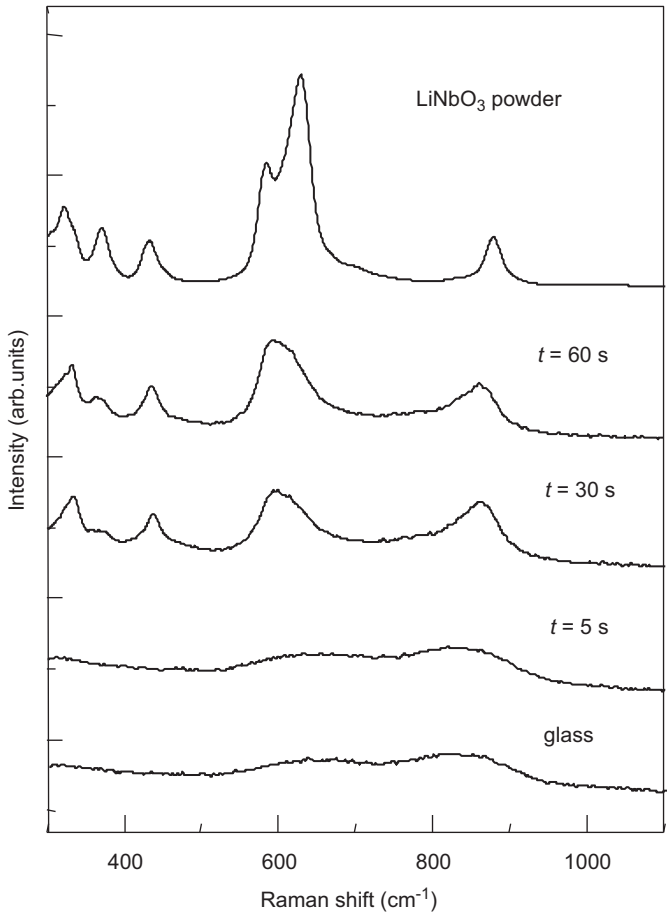

Fig. 3. Micro-Raman scattering spectra at room temperature for dots patterned by Nd:YAG laser irradiations for the Cu–LNS glass. The data for the base Cu–LNS glass (no laser irradiations) and $LiNbO_3$ crystal powders are also shown.

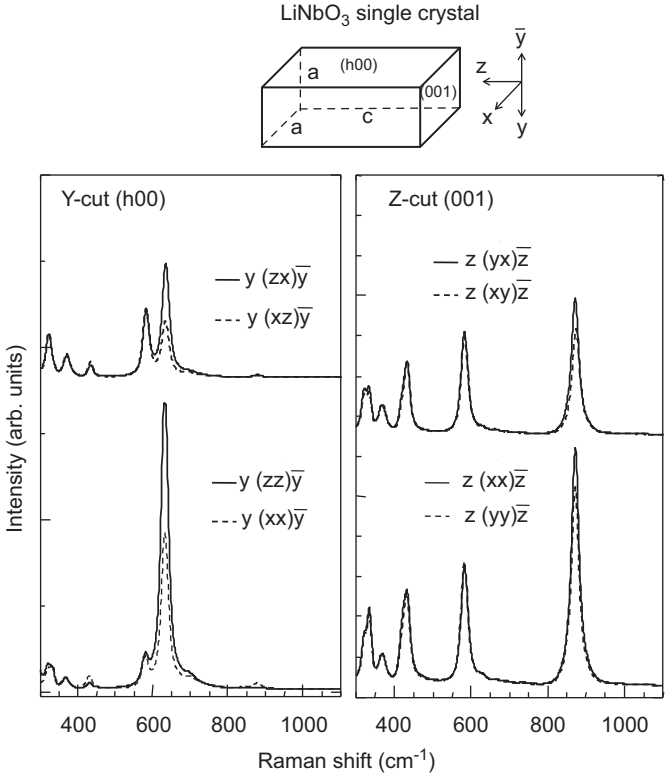

Fig. 4. Linearly polarized Raman scattering spectra at room temperature for Y- and Z-cut $LiNbO_3$ single crystals commercially available.

the laser power of $P=0.7$ W. These results indicate that laser irradiations with $P>0.5$ W and $t>30$ s induce the formation of $LiNbO_3$ crystals.

In order to clarify the orientation and growth mechanism of $LiNbO_3$ crystals, in the laser-irradiated part, we carried out linearly polarized micro-Raman scattering experiments for the dots. For the analysis and reference of Raman scattering spectra, we first measured the linearly polarized Raman scattering spectra for *Y*-cut and *Z*-cut $LiNbO_3$ single crystals being commercially available, and the data are shown in Fig. 4. It is seen that the Raman spectrum, i.e., the peak position and intensity, changes largely depending on the crystal plane. The Raman scattering spectra for $LiNbO_3$ single crystals have been reported by several authors [31–34], and all Raman bands shown in Fig. 4 are attributed to bending and stretching vibrations related to Nb–O bonds in an $LiNbO_3$.

The polarized optical microscope (POM) observations for the surface and cross-section of the dot obtained by LD laser irradiations of $P=1.4$ W and $t=20$ s are shown in Fig. 5. Here, LD laser was used, because the absorption coefficient of $\alpha=7.19\ cm^{-1}$ at $\lambda=795$ nm is large compared with Nd:YAG laser and dots with large sizes are

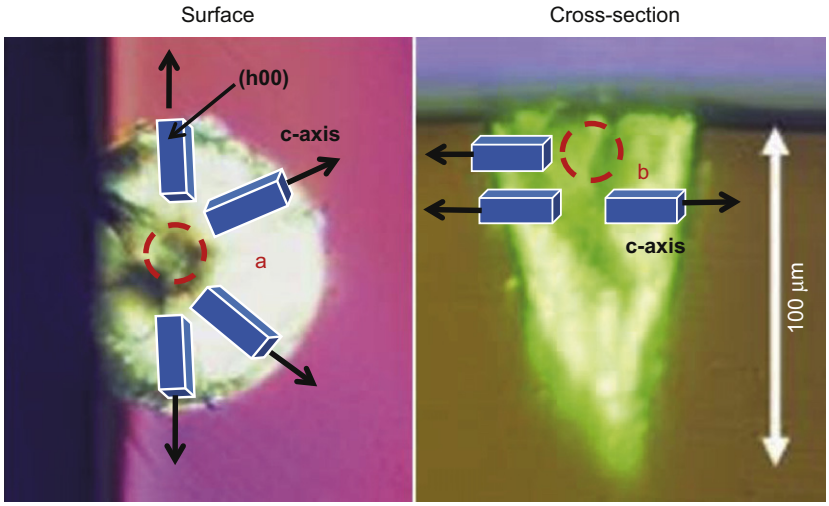

Fig. 5. Polarized optical microscope observations for the surface and cross-section of the dot obtained by LD laser ($\lambda=795$ nm) irradiations of $P=1.4$ W and $t=20$ s in the Cu–LNS glass. Schematic model for the orientation of $LiNbO_3$ crystals at the edge parts of the surface and cross-section of the dot is also shown.

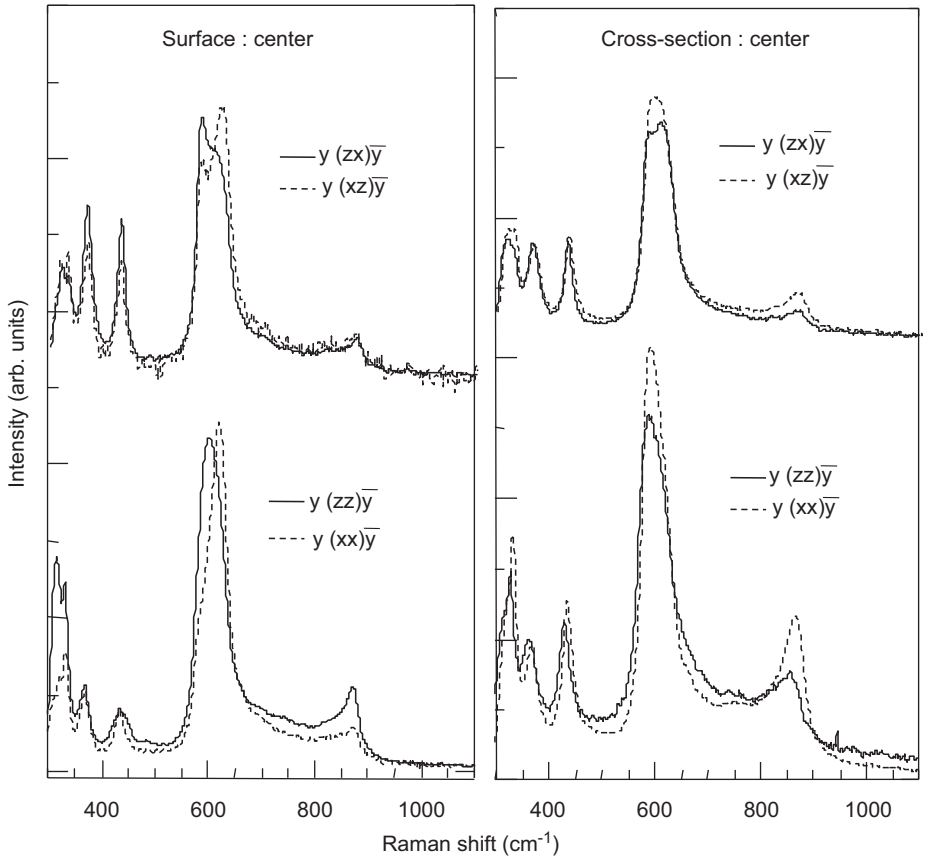

Fig. 6. Linearly polarized micro-Raman scattering spectra at room temperature for the center part of the surface and cross-section of the dot shown in Fig. 5.

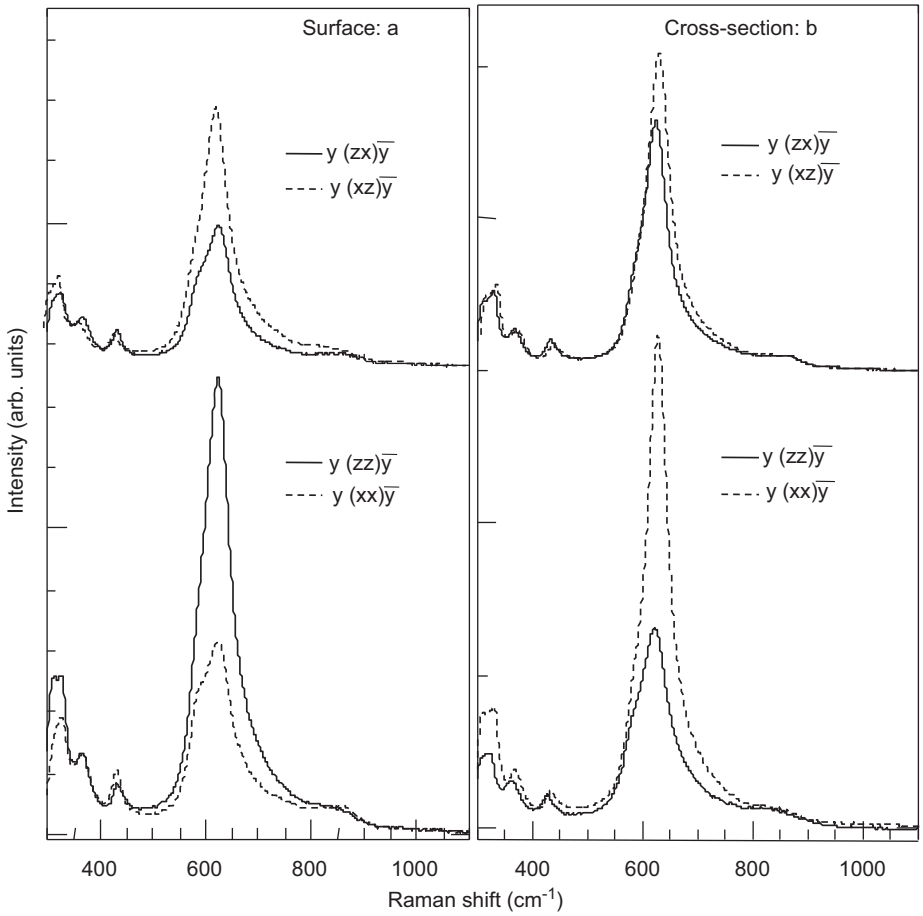

Fig. 7. Linearly polarized micro-Raman scattering spectra at room temperature for the edge parts of the surface (a) and the cross-section (b) of the dot shown in Fig. 5.

obtained. As can be seen in Fig. 5, the surface diameter of dots is about 70 μm and the depth length in the cross-section is about 100 μm. It would be possible to examine the orientation of $LiNbO_3$ crystals more clearly in such a dot with a large size. The positions for micro-Raman scattering spectrum measurements are marked in the figure, and the data obtained are shown in Figs. 6 and 7. For the center parts of the surface and cross-section of the dot, the Raman spectra change depending on polarization directions, but from the comparison with the data of $LiNbO_3$ single crystals (Fig. 4), it is obvious that the Raman spectra include both features corresponding to the (h 0 0) and (0 0 l) planes. In particular, it is also noted that the band at 870 cm^{-1} being typical for the (0 0 l) plane is observed in the configuration of $y(zz)\bar{y}$. Therefore, the spectra shown in Fig. 6 suggest that the orientation degree of $LiNbO_3$ crystals at the center parts of the surface and cross-section of the dot is not good, might be close to the random orientation.

For the edge parts of the surface and cross-section of the dot, it is observed that the intensity of the peak at 630 cm^{-1} changes largely, depending on the configuration of $y(zz)\bar{y}$ and $y(xx)\bar{y}$ and the peak intensity at 870 cm^{-1} is very small. These spectra are similar to those for the (h 0 0) plane of $LiNbO_3$ single crystal (Fig. 4), suggesting strongly that $LiNbO_3$ crystals are oriented highly at the edge parts of the surface and cross-section of the dot, i.e., the c-axis orientation. The schematic model for the orientation of $LiNbO_3$ crystals at the edge parts of the surface and cross-section of the dot patterned by laser irradiations in Cu–LNS glass is shown in Fig. 5.

Because the Cu–LNS glass has the values of T_g=544 and T_p=692 °C, the temperature of the center of dots giving the formation of $LiNbO_3$ crystals would be close to or higher than T_p=692 °C. With an increasing laser irradiation time, the temperature profile (distribution) in the laser-irradiated region would change and the temperature increase at the center of dots would be expected. And, it should be pointed out that the temperature gradient is created in the laser-irradiated region. The creation of temperature gradient in the heating by laser irradiations is different from the case of usual heat treatment in an electric furnace giving a homogeneous temperature distribution over a whole part of glass. The temperature gradient in the laser-irradiated part would be an important reason for the formation of oriented $LiNbO_3$ crystals in dots. The results of the Raman scattering spectra, shown in Figs. 6 and 7, indicate that the preferential crystal growth direction of an $LiNbO_3$ in the laser-irradiated region is the c-axis.

As shown in Fig. 2, the sinkings were formed at the surrounding of dots. This behavior is interpreted as follows. In the initial laser irradiations with short irradiation times, the temperature of the laser-irradiated region increases, consequently giving the volume expansion. The crystallization of $LiNbO_3$ is taking place in the laser irradiations with prolonged irradiation times. Because the densities of Cu–LNS glass and $LiNbO_3$ are 3.771 and 4.648 g/cm^3, respectively, it is expected that the volume contraction would occur with the formation of $LiNbO_3$ crystals.

3.3. Growth of $LiNbO_3$ crystal lines by laser irradiation

The POM and CSLM photographs for the sample obtained by Nd:YAG laser (λ=1064 nm) irradiations with P=0.65 W and S=5 μm/s in Cu–LNS glass are shown in Fig. 8. It was confirmed from micro-Raman scattering spectra that $LiNbO_3$ crystals are formed in the laser-irradiated part. As can be seen in Fig. 8, the line width is

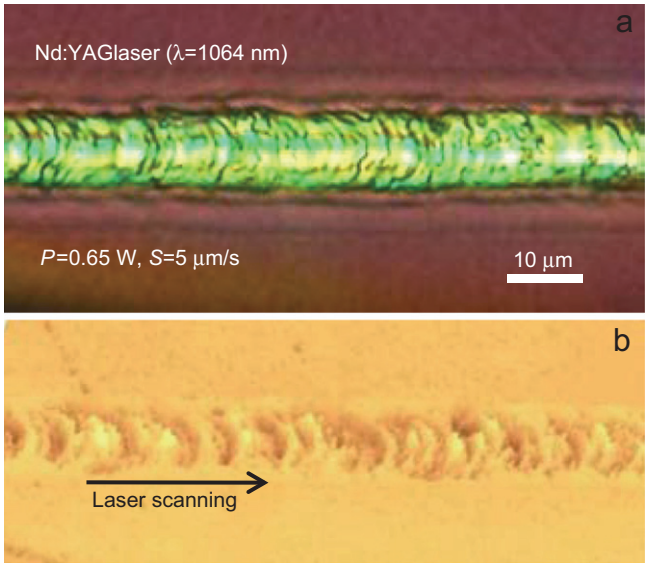

Fig. 8. Polarized optical and confocal scanning laser microscope photographs for the sample obtained by Nd:YAG laser (λ=1064 nm) irradiations with P=0.65 W and S=5 μm/s in the Cu–LNS glass.

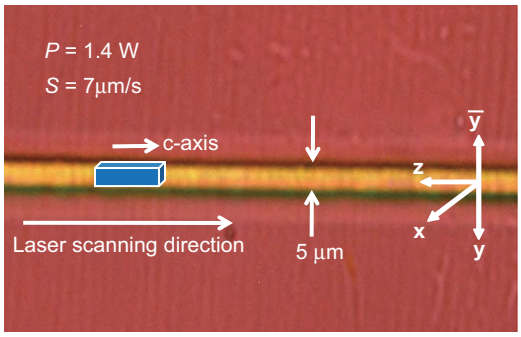

Fig. 9. Polarized optical microscope photograph for the sample obtained by Yb:YVO_4 laser (λ=1080 nm) irradiations with P=1.4 W and S=7 μm/s in the Cu–LNS glass.

about 10 μm and the surface morphology is not homogeneous. We tried Nd:YAG laser irradiations with different power and scanning speed conditions, but it was difficult to pattern $LiNbO_3$ crystal lines with a homogeneous morphology.

The POM micrograph for the sample obtained by Yb:YVO_4 laser (λ=1080 nm) irradiations with P=1.4 W and S=7 μm/s in the Cu–LNS glass is shown in Fig. 9. It is seen that a line with a homogeneous surface morphology is patterned. It was confirmed from the SHG microscope observations that the line shows SHGs. With a configuration shown in Fig. 9, the linearly polarized micro-Raman scattering spectra were measured for the surface and cross-section of this line, and the results are shown in Fig. 10. From the comparison with the Raman spectra for Y- and Z-cut $LiNbO_3$ single crystal, it is obvious that an $LiNbO_3$ being present in the line is highly oriented. In particular, it is concluded that the growth direction of an $LiNbO_3$ along the laser scanning direction is the c-axis. It should be pointed out that the growth direction of the c-axis in $LiNbO_3$ crystal lines is the same as that in the dots shown in Fig. 5. Recently, Honma et al. [13,14] tried to pattern $LiNbO_3$ crystal lines in different glass compositions such as $0.5CuO–40Li_2O–32Nb_2O_5–28SiO_2$, $0.5CuO–0.5Er_2O_3–40Li_2O–32Nb_2O_5–28SiO_2$, and $5Sm_2O_3–35Li_2O–30Nb_2O_5–20SiO_2–15B_2O_3$ using Yb:YVO_4 fiber laser (λ=1080 nm) irradiations and reported that $LiNbO_3$ crystals with the c-axis orientation are formed along the laser scanning direction. They also confirmed that light is confined in $LiNbO_3$ crystal lines (i.e., work as optical waveguide) and Er^{3+} ions are incorporated into $LiNbO_3$ lines patterned by laser irradiations [13,14].

In the laser scanning, the maximum temperature moves along the laser scanning direction. That is, the profile of the temperature distribution changes also with time. It is obvious that the matching of the crystal growth rate of an $LiNbO_3$ in a given glass and the laser scanning speed is an important factor for the constant growth of an $LiNbO_3$ in the laser-irradiated region. If the matching between them is not satisfied, the surface morphology of lines would not be smooth. The glass composition of a given precursor glass would also be important for crystal patterning by laser irradiations, because the crystal growth rate changes depending on the glass composition. Indeed, Honma et al. [13] reported the laser patterning of inhomogeneous $LiNbO_3$ crystal lines in the $0.5CuO–35Li_2O–30Nb_2O_5–35SiO_2$ glass with a large amount (35 mol%) of network former SiO_2.

In order to pattern lines consisting of highly oriented $LiNbO_3$ crystals, the crystal nucleation at the laser-irradiated part has to be avoided. In Nd:YAG laser irradiations, lines with broad widths are patterned compared with Yb:YVO_4 fiber laser irradiation, as shown in Figs. 8 and 9. In the case of laser irradiations with broad areas, the temperature gradient in the laser-irradiated region would be gentle, and the change in temperature during laser scanning would be small. The probability of the crystal nucleation would be large in such broad laser-irradiated part, consequently giving the patterning of crystal lines with inhomogeneous surface morphology. Similar phenomena have been observed in the laser patterning of nonlinear optical $Sm_xBi_{1-x}BO_3$ crystals with Nd:YAG laser in $Sm_2O_3–Bi_2O_3–B_2O_3$ glasses, in which the crystal lines with rough surface morphologies are patterned in conditions giving broad laser-irradiated areas [2,35]. Recently, Honma et al. [13–15] reported the patterning of line- and planar-shape $LiNbO_3$ crystals with a high orientation, in which Yb:YVO_4 fiber lasers with λ=1080 nm have been used. Therefore, it is proposed that lasers being available to give small focusing areas such as Yb:YVO_4 fiber lasers are better for the patterning of homogeneous crystal lines.

For photonic device applications of laser-patterned $LiNbO_3$ crystals such as tunable optical switching, lines consisting of highly oriented $LiNbO_3$ crystals, like single crystal $LiNbO_3$ lines, are strongly required. In the present study, cw-type lasers have been used, and the patterning of $LiNbO_3$ crystal lines with a preferential growth direction has been succeeded. Yonezaki et al. [36] succeeded in crystallizing $LiNbO_3$ crystals by near-infrared femtosecond (fs) laser irradiations in $32.5Li_2O–27.5Nb_2O_5–40SiO_2$ glass. But, there have been no reports on the patterning of highly oriented $LiNbO_3$ crystal lines by using fs lasers. Considering the complicated mechanism (process) of structural modifications in glass by fs laser irradiations [36], the morphology of crystals patterned by fs and cw laser irradiations would be expected to differ. It is obvious that the profile of the temperature distribution in the laser-irradiated region and its change along laser scanning would be one of the most important conditions for the patterning of highly oriented crystals. Very recently, Stone et al. [37] succeeded in patterning of $LaBGeO_5$ crystals in an $LaBGeO_5$ glass by the fs laser (λ=800 nm) irradiations. They reported that crystal lines written with fs laser had glass remaining at the center, which was absent with the cw laser. They also stated that such differences likely arise from substantial differences in the temperature gradients between the two (fs and cw lasers) methods [37].

As demonstrated in the present study, by selecting the type of cw laser, the degrees of laser power, irradiation time, and scanning speed, dots and lines consisting of $LiNbO_3$ crystals with a preferential growth orientation have been patterned. So far, the present authors' group has reported the line patterning of several crystals using cw laser irradiations, in which nonlinear optical and lithium ion conductive crystals such as β-BaB_2O_4, $Ba_2TiGe_2O_8$, β′-$Gd_2(MoO_4)_3$,

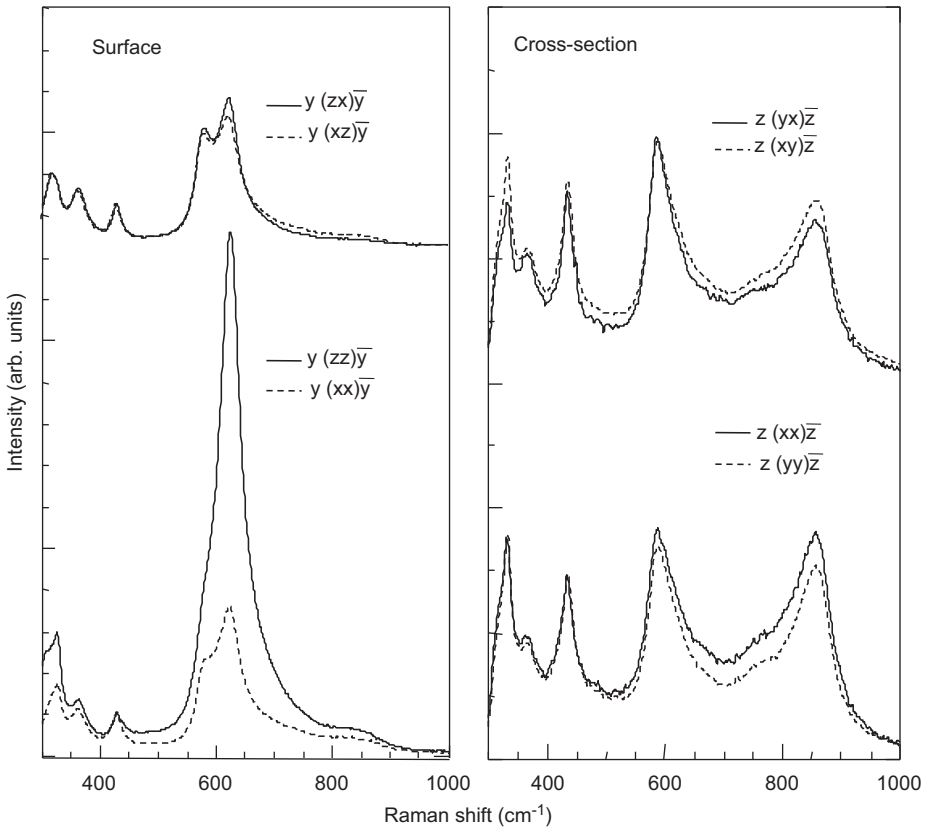

Fig. 10. Linearly polarized micro-Raman scattering spectra at room temperature for the surface and cross-section of the line shown in Fig. 9.

$Ba_3Ti_3O_6(BO_3)_2$, $Li_2Si_2O_5$, and $LiFePO_4$ show preferential growth orientations in the patterned lines [2,3,7–9,11,13–15,38–41]. It is, therefore, emphasized that the laser-induced crystallization is regarded as a conventional and versatile technique for the patterning of crystals with high growth orientation in oxide glasses.

4. Conclusions

The dots and lines consisting of $LiNbO_3$ crystals were patterned on the surface of $1CuO–40Li_2O–32Nb_2O_5–28SiO_2$ glass by irradiations of continuous-wave Nd:YAG laser (wavelength: $\lambda=1064$ nm), diode laser ($\lambda=795$ nm), and Yb:YVO_4 fiber laser ($\lambda=1080$ nm), and the feature of laser-patterned $LiNbO_3$ crystal growth was examined from linearly polarized micro-Raman scattering spectrum measurements. It was found that the *c*-axis orientation of $LiNbO_3$ crystals is taking place in both dots and lines. It is proposed that the temperature gradient in the laser-irradiated region induces a preferential growth orientation and laser irradiation giving a narrow width is one of the important factors for the patterning of $LiNbO_3$ crystal lines with homogeneous surface morphologies.

Acknowledgments

This work was supported by the Grant-in-Aid for Scientific Research from the Ministry of Education, Science, Sports, Culture and Technology, Japan, and partly by the Program for Developing the Supporting System for Global Multidisciplinary Engineering Establishment in the Nagaoka University of Technology. We also thank to Dr. Ralf Mueller for valuable discussions on the laser-induced crystallization.

References

[1] M.C. Gower, Opt. Express 7 (2000) 56.
[2] T. Honma, Y. Benino, T. Fujiwara, T. Komatsu, Appl. Phys. Lett. 88 (2006) 231105.
[3] T. Komatsu, R. Ihara, T. Honma, Y. Benino, R. Sato, H.G. Kim, T. Fujiwara, J. Am. Ceram. Soc. 90 (2007) 699.
[4] B. Franta, T. Williams, C. Faris, S. Feller, M. Affatigao, Phys. Chem. Glasses: Eur. J. Glass Sci. Technol. B 48 (2007) 357.
[5] Y. Dai, B. Zhu, J. Qiu, H. Ma, B. Lu, B. Yu, Chem. Phys. Lett. 443 (2007) 253.
[6] P. Gupta, H. Jain, D.B. Williams, T. Honma, Y. Benino, T. Komatsu, J. Am. Ceram. Soc. 91 (2008) 110.
[7] T. Honma, J. Ceram., Soc. Jpn. 118 (2010) 71.
[8] T. Honma, Y. Benino, T. Fujiwara, T. Komatsu, R. Sato, Appl. Phys. Lett. 83 (2003) 2796.
[9] R. Ihara, T. Honma, Y. Benino, T. Fujiwara, R. Sato, T. Komatsu, Solid State Commun. 136 (2005) 273.
[10] K. Koshiba, T. Honma, Y. Benino, T. Komatsu, Appl. Phys. A 89 (2007) 981.
[11] Y. Tsukada, T. Honma, T. Komatsu, Appl. Phys. Lett. 94 (2009) 059901.
[12] H. Sugita, T. Honma, Y. Benino, T. Komatsu, Solid State Commun. 143 (2007) 280.
[13] T. Honma, K. Koshiba, Y. Benino, T. Komatsu, Opt. Mater. 31 (2008) 315.
[14] T. Honma, T. Komatsu, D. Zhao, H. Jain, IOP Conf. Ser.: Mater. Sci. Eng. 1 (2009) 012006.
[15] T. Honma, T. Komatsu, Opt. Express 18 (2010) 8019.
[16] T. Komatsu, H. Tawarayama, H. Mohri, K. Matusita, J. Non-Cryst. Solids 135 (1991) 105.
[17] H.G. Kim, T. Komatsu, R. Sato, K. Matusita, J. Non-Cryst. Solids 162 (1993) 201.
[18] Y. Ding, A. Osaka, Y. Miura, H. Toratani, Y. Matsuoka, J. Appl. Phys. 77 (1995) 2208.
[19] M. Todorovic, Lj. Radonjic, Ceram. Int. 23 (1997) 55.
[20] H. Jain, Ferroelectrics 306 (2004) 111.
[21] Y. Hu, C.L. Huang, J. Non-Cryst. Solids 278 (2000) 170.
[22] N.S. Prasad, K.B.R. Varma, J. Non-Cryst. Solids 351 (2005) 1455.
[23] M.P.E. Graca, M.G.F. Silva, A.S.B. Sombra, M.A. Valente, J. Non-Cryst. Solids 353 (2007) 4390.
[24] V.N. Sigaev, N.V. Golubev, S.Yu. Stefanovich, T. Komatsu, Y. Benino, P. Pernice, A. Aronne, E. Fanelli, B. Champagnon, V. Califano, D. Vouagner, T.E. Konstantinova, V.A. Glazunova, J. Non-Cryst. Solids 354 (2008) 873.
[25] N.V. Golubev, V.N. Sigaev, S.Yu. Stefanovich, T. Honma, T. Komatsu, J. Non-Cryst. Solids 354 (2008) 1909.
[26] P. Prapitpongwanich, K. Pengpat, C. Russel, Mater. Chem. Phys. 113 (2009) 913.
[27] T. Honma, D. Oku, T. Komatsu, Solid State Ionics 180 (2009) 1457.

[28] R.P.S. Chakradhar, B. Yasoda, J.L. Rao, N.O. Gopal, J. Non-Cryst. Solids 352 (2006) 3864.
[29] R. Debnath, S.K. Das, Chem. Phys. Lett. 155 (1989) 52.
[30] R.F. Schaufele, M.J. Weber, Phys. Rev. 152 (1966) 705.
[31] A. Duran, J.M.F. Navarro, Phys. Chem. Glasses 26 (1985) 126.
[32] R. Claus, G. Borstel., E. Wiesendanger, L. Steffan, Phys. Rev. B 6 (1972) 4878.
[33] H.R. Xia, S.Q. Sun, X.F. Cheng, S.M. Dong, H.Y. Xu, L. Gao, D.L. Cui, J. Appl. Phys. 98 (2005) 033513.
[34] P. Galinetto, M. Marinone, D. Grando, G. Samoggia, F. Caccavale, A. Morbiato, M. Musolino, Opt. Laser Eng. 45 (2007) 380.
[35] T. Honma, Y. Benino, T. Fujiwara, T. Komatsu, J. Am. Ceram. Soc. 88 (2005) 989.
[36] Y. Yonesaki, K. Miura, R. Araki, K. Fujita, K. Hirao, J. Non-Cryst. Solids 351 (2005) 885.
[37] A. Stone, M. Sakakura, Y. Shimotsuma, G. Stone, P. Gupta, K. Miura, K. Hirao, V. Dierolf, H. Jain, J. Non-Cryst. Solids 356 (2010) 3059.
[38] K. Hirose, T. Honma, Y. Benino, T. Komatsu, Solid State Ionics 178 (2007) 801.
[39] T. Honma, P.T. Nguyen, T. Komatsu, J. Ceram. Soc. Jpn. 116 (2008) 1314.
[40] T. Oikawa, T. Honma, T. Komatsu, Cryst. Res. Technol. 43 (2008) 1253.
[41] T. Honma, T. Komatsu, Y. Benino, J. Mater. Res. 23 (2008) 885.